In vitro evaluation of protein–protein interactions in the rice KAI2 ligand signaling complex

Keita Tanaka[1,2], Jiawang Wu[1,2], Yutaro Harada[3], Taiki Suzuki[3], Yujiao Yan[1,2], Yoshiya Seto[3], Hiromu Kameoka[1,2,*]

1. Key Laboratory of Plant Carbon Capture, CAS Centre for Excellence in Molecular Plant Sciences, Chinese Academy of Sciences, 300 Fenglin Road, Shanghai 200032, China.
2. CAS-JIC Centre of Excellence for Plant and Microbial Science (CEPAMS), Center for Excellence in Molecular Plant Sciences, Chinese Academy of Sciences, 300 Fenglin Road, Shanghai 200032, China.
3. Laboratory of Plant Chemical Regulation, School of Agriculture, Meiji University, 1-1-1 Higashi-Mita, Tama-ku, Kawasaki, Kanagawa 214-8571, Japan.

*: corresponding author

Contact: khiromu@cemps.ac.cn

Running title: Protein–protein interactions in the rice KL signaling complex

Abstract

KARRIKIN INSENSITIVE 2 (KAI2)/DWARF14-LIKE (D14L) plays key roles in land plant development, environmental responses, and the establishment of arbuscular mycorrhizal symbiosis, likely acting as the receptor for unidentified signaling molecules termed KAI2-ligands (KLs). KL perception by KAI2/D14L promotes DWARF3 (D3)/MORE AXILLARY GROWTH2 (MAX2) F-box protein-mediated ubiquitination of SUPPRESSOR OF MAX2 1 (SMAX1) proteins, thereby transducing the KL signals. Although genetic and *in vivo* assays have demonstrated the functions of these components, the biochemical details of their interactions remain elusive. Here we investigated physical interactions between rice D14L, D3, and OsSMAX1 *in vitro* using desmethyl germinone (dMGer), a recently developed KL analog. dMGer elicited KL responses in rice with higher activity and pathway specificity than a widely used KL analog (−)-GR24. dMGer, but not (−)-GR24, directly bound to D14L and promoted the interaction between D14L and D3 *in vitro*. The interaction between D14L and OsSMAX1 was also enhanced by dMGer. Furthermore, we identified the domain of OsSMAX1 that distinguishes it from its paralog DWARF53 (D53), which is associated with the strigolactone signaling complex. These findings propose a model of the interactions among KL signaling components and highlight the role of the ligand in the signaling complex.

Keywords: KARRIKIN INSENSITIVE2 (KAI2)/DWARF14-LIKE (D14L), DWARF3 (D3)/MORE AXYLLARY GROWTH2 (MAX2), SUPPRESSOR OF MAX2 1 (SMAX1), KAI2 ligand (KL), desmethyl germinone (dMGer), protein–protein interaction

Introduction

The α/β-fold hydrolase KARRIKIN INSENSITIVE2 (KAI2)/DWARF14-Like (D14L) is conserved in land plants and regulates diverse aspects of their life cycles. *KAI2* was first identified in *Arabidopsis thaliana* (Arabidopsis) as a gene essential for the response to karrikins (KARs), a group of smoke-derived butenolides that stimulate seed germination and photomorphogenesis (Chiwocha et al., 2009; Waters et al., 2012a). *KAI2*/*D14L* regulates not only seed germination and photomorphogenesis but also root development (Villaécija-Aguilar et al., 2019; Carbonnel et al., 2020; Meng et al., 2022), drought response (Li et al., 2017), arbuscular mycorrhizal (AM) symbiosis (Gutjahr et al., 2015), etc. Notably, KARs are absent in living plants, whereas *kai2*/*d14l* mutants exhibit phenotypes opposite to those induced by KAR treatment in wild-type (WT) plants. For example, KAR treatment suppresses mesocotyl elongation in *Oryza sativa* (rice) in the dark, whereas *d14l* mutants exhibit elongated mesocotyls (Gutjahr et al., 2015; Zheng et al., 2020). These findings suggest that KAI2/D14L mediates responses to an unidentified endogenous compound distinct from KARs. Since KAI2/D14L is considered to be its receptor, this putative compound is referred to as KAI2 ligand (KL) (Conn and Nelson, 2016).

The KL signaling pathway is composed of components of the strigolactone (SL) signaling pathway or their paralogs. In SL signaling, SLs bind to DWARF14 (D14)/DECREASED APICAL DOMINANCE2/RAMOSUS3, a paralog of KAI2/D14L, promoting the interaction of D14 with the F-box protein MORE AXILLARY GROWTH2 (MAX2)/DWARF3 (D3) in an Skp, Cullin, F-box (SCF) complex. D14 also interacts with the repressor of the SL signal, DWARF53 (D53) in rice or SUPPRESSOR OF MAX2 1 (SMAX1)-LIKE6/7/8 (SMXL6/7/8) in Arabidopsis, in an SL-dependent manner (Jiang et al., 2013; Zhou et al., 2013; Wang et al., 2015; Wang et al., 2020a; Soundappan et al.). SLs thus trigger the formation of a D14-$SCF^{MAX2/D3}$-D53/SMXL6/7/8 complex and subsequent ubiquitination and 26S-proteasomal degradation of the repressor D53/SMXL6/7/8 proteins, thereby inducing SL responses. On the other hand, in KL signaling, KL is considered to be perceived by KAI2/D14L, which triggers the formation of the KAI2/D14L–$SCF^{MAX2/D3}$–SMAX1/SMXL2/OsSMAX1 complex and their degradation.

The functions of the domains of these components have also been investigated. SMXL proteins contain conserved domains, N-terminal domain (N), putative ATPase domain 1 (D1), middle region (M), and C-terminal putative ATPase domain 2 (D2). The D2 domain is required for MAX2/D3-mediated degradation (Jiang et al., 2013; Zhou et al., 2013; Wang et al., 2020b;

Khosla et al., 2020). Yeast two-hybrid assays have shown that the D1, or D1 and M (D1M) domains are responsible for the ligand-dependent interaction with D14 or KAI2/D14L (Zhou et al., 2013; Khosla et al., 2020). In addition, the D53-D2 domain interacts with D14 in a ligand and C-terminal α-helix of D3 (D3-CTH)-dependent manner (Shabek et al., 2018). D3-CTH affects ligand hydrolysis by KAI2 and SMAX1 ubiquitination. Furthermore, MAX2 lacking CTH did not complement the KL-related phenotypes in the *max2* mutants. These results suggest the involvement of D3-CTH in KL signaling (Tal et al., 2023). However, its role in the interactions of the KL signaling components remains unclear.

Although the natural KL has not been identified, *in vivo* co-immunoprecipitation assays and yeast two-hybrid assays using KAR or artificial KL analogs demonstrated the interactions of the KL signaling components triggered by the ligands (Khosla et al., 2020; Zheng et al., 2020; Yao et al., 2021b; Okabe et al., 2023); however, the evidence for direct interactions between these components, in other words, *in vitro* proof of their interactions, is still limited. In Arabidopsis, *in vitro* interaction between KAI2 and SMAX1 has not been shown. Although a report shows that KAI2 and MAX2 slightly interact with each other in a ligand-dependent manner, the interaction is much weaker than that between AtD14 and MAX2 detected under the same conditions (Xu et al., 2018). In rice, *in vitro* interaction between D14L and D3 has not been shown. The interaction between D14L and OsSMAX1 has been reported (Zheng et al., 2020); however, its ligand dependency has not been demonstrated.

A possible reason for the limited evidence of the *in vitro* interaction is insufficient activation of KAI2/D14L by KAR or artificial KL analogs. Differential scanning fluorimetry (DSF) has been used to evaluate the activity of the putative ligands of D14 or KAI2/D14L, in which the shifts in thermal stability (melting temperature; Tm) of the proteins indicate structural changes induced by ligand binding (Niesen et al., 2007). Previous works suggest that not ligand binding alone but the shift in receptor stability in DSF is the better indicator of ligand activity (Seto et al., 2019; Kushihara et al., 2025). Natural SLs and (+)-GR24, an artificial SL analog, induce large shifts towards destabilization of D14 (Hamiaux et al., 2012; Abe et al., 2014; de Saint Germain et al., 2016; Seto et al., 2019; Yao et al., 2021b) (Supplemental Figure 1). On the other hand, KARs do not induce shifts in KAI2/D14L (Waters et al., 2015; Fukui et al., 2019). This result has raised a hypothesis that the direct ligands of KAI2/D14L are not KARs themselves, but uncharacterized metabolite(s) derived from KARs in plants. Interestingly, (−)-GR24 (Supplementary Figure 1), a widely used artificial KL analog, induces only slight shifts in KAI2 stability in Arabidopsis (Fukui et al., 2019; Yao et al., 2021b).

Moreover, it does not induce shifts in some species, including rice, *Brachypodium distachyon*, and *Selaginella moellendorffii* (Waters et al., 2015; Yao et al., 2021a; Meng et al., 2022). These results suggest the possibility that (−)-GR24 does not possess sufficient activity to enhance the interactions between the KL signaling components.

Recently, a new type of compounds, desmethyl butenolides, has been reported to function as KL analogs (Yao et al., 2021b). While natural SLs, artificial SL analogs, and (−)-GR24 have a methyl group on their butenolide ring, desmethyl-type KL analogs lack this methyl group. Currently, four types of desmethyl-type KL analogs, desmethyl Yoshimulactone Green (dYLG, Supplemental Figure 1), desmethyl-GR24 (dGR24), desmethyl-CN-debranone, and desmethyl germinone (dMGer, Supplemental Figure 1), have been developed (Yao et al., 2018; Yao et al., 2021b; Okabe et al., 2023). dYLG binds to the ligand binding pocket of KAI2/D14L and emits fluorescence upon hydrolysis by KAI2/D14L. The other three compounds have been shown to induce stronger KL responses *in vivo* and larger stability shifts of KAI2/D14L in DSF than (−)-GR24 (Yao et al., 2021b; Meng et al., 2022; Okabe et al., 2023; Kushihara et al., 2025). dMGer reportedly induces the interaction between Arabidopsis KAI2 and SMAX1 in yeast two-hybrid assays (Okabe et al., 2023; Kushihara et al., 2025). However, whether desmethyl butenolide-type ligands can induce the interactions of the KL signaling components *in vitro* has not yet been examined.

Here, we revisit the rice KL signaling using artificial KL analogs, (−)-GR24 and dMGer. Pharmacological assays reveal that dMGer activates the KL signaling pathway more strongly and specifically than (−)-GR24. *In vitro* assays demonstrate direct recognition of dMGer by D14L. We evaluate the interactions between D14L, D3, and OsSMAX1, providing direct evidence for the enhancement of D14L–D3 and D14L–OsSMAX1 interactions by dMGer. Furthermore, by assaying the interactions among D14L, D14, and domains of OsSMAX1 and D53, we reveal the functions of the domains that underlie the specific interactions of D14L–OsSMAX1 and D14–D53. Thus, our study refines the biochemical understanding of the KL signaling pathway.

Results

dMGer induces KL responses in rice

140 While the activities of desmethyl-type KL analogs have been assessed with D14L/KAI2 from
141 several species *in vitro*, their KAI2/D14L-dependent activities *in vivo* have been examined only
142 in Arabidopsis. dMGer, a recently developed desmethyl-type KL analog, promotes seed
143 germination and inhibits hypocotyl elongation in Arabidopsis in a KAI2-dependent manner
144 (Okabe et al., 2023; Kushihara et al., 2025). To evaluate the activities of dMGer as a KL analog,
145 we examined the responses of rice to dMGer.

146 We first assessed the dMGer activity on mesocotyl length. Elongation of mesocotyls in
147 dark-grown rice seedlings is a well-characterized phenotype regulated by the KL signaling
148 pathway (Kameoka and Kyozuka, 2015; Gutjahr et al., 2015; Choi et al., 2020; Zheng et al.,
149 2020). *d14l* mutants exhibit longer mesocotyls than WT, whereas KARs and (−)-GR24
150 suppress mesocotyl elongation in a *D14L*-dependent manner (Zheng et al., 2020). We
151 compared mesocotyl length of seedlings grown in the dark with or without 1 μM dMGer
152 treatment. WT seedlings treated with dMGer developed shorter mesocotyls than those of the
153 control group (Figure 1A and 1B). In contrast to WT seedlings, *d14l* seedlings showed no
154 significant difference in mesocotyl length between dMGer-treated and untreated groups
155 (Figure 1A and 1B). These results indicate that dMGer suppresses mesocotyl elongation
156 through the KL signaling pathway in rice.

157 To further characterize the activity of dMGer in rice, we analyzed transcriptional responses
158 of KL-responsive markers, *D14-LIKE2b* (*DLK2b*) (Os01g0595600) and *KARRIKIN-UP-*
159 *REGULATED F-BOX1* (*KUF1*) (Os06g0711700), to dMGer treatment, comparing them with
160 those induced by (−)-GR24. Previous studies have shown that, across land plant species,
161 homologues of these genes are induced by the KL signals (Waters et al., 2012b; Choi et al.,
162 2020; Zheng et al., 2020; Mizuno et al., 2021; Sepulveda et al., 2022; Meng et al.). In WT
163 seedlings, dMGer induced the expression of *DLK2b* (Figure 1C) and *KUF1* (Figure 1D) in a
164 dose-dependent manner. While 1 μM and 10 μM dMGer significantly induced *DLK2b*, only
165 10 μM (−)-GR24 induced it under our experimental conditions (Figure 1C). Similarly, *KUF1*
166 was induced by 1 μM dMGer but was unchanged by (−)-GR24 at the same concentration.
167 These results indicate that dMGer induces stronger transcriptional activation of KL-responsive
168 markers in rice than (−)-GR24. To determine whether these responses require *D14L*, we
169 examined the responses in *d14l* mutant seedlings. In *d14l*, 10 μM dMGer did not induce either
170 *DLK2b* (Figure 1E) or *KUF1* (Figure 1F). In contrast, 10 μM (−)-GR24 strongly induced
171 *DLK2b* (Figure 1E). The expression of *KUF1* also tended to be induced by (−)-GR24 (Figure

172 1F). These results indicate that dMGer activity in rice depends on D14L, whereas (−)-GR24
173 can also act through D14L-independent pathways. Together, these results demonstrate the *in*
174 *vivo* dMGer functions as an effective and selective KL analog in rice.

175

176 **dMGer binds to D14L and induces its structural changes *in vitro***

177 We then examined whether dMGer directly interacts with D14L. We first conducted dYLG
178 (Supplemental Figure 1) assays. dYLG is hydrolyzed in the ligand-binding pocket of
179 D14L/KAI2 and releases a fluorophore. In this assay, the test compounds and dYLG are co-
180 incubated with recombinant D14L/KAI2. Test compounds that bind to the ligand-binding
181 pocket of D14L/KAI2 reduce the fluorescence of the dYLG-derived fluorophore by
182 competitively inhibiting the hydrolysis of dYLG. D14L was incubated with 1 μM dYLG and
183 different concentrations of dMGer or (−)-GR24. dMGer significantly reduced dYLG
184 hydrolysis at 1 μM and almost completely abolished it at 5–10 μM (Figure 2A). By contrast,
185 (−)-GR24 did not affect dYLG hydrolysis even at 10 μM. These results suggest that dMGer,
186 but not (−)-GR24, binds to the ligand binding pocket of D14L.

187 We also examined the binding of these compounds to D14L using DSF. D14L showed no
188 Tm shift upon addition of (−)-GR24 (Figure 2B). In contrast, D14L showed a clear, dose-
189 dependent decrease in Tm upon addition of dMGer (Figure 2B), indicating the ability of dMGer
190 to directly interact with and change the structure of D14L.

191

192 **dMGer enhances the direct interactions of D14L with D3 and OsSMAX1**

193 We next examined the interactions between the KL signaling components *in vitro*. We first
194 performed pull-down assays using maltose-binding protein (MBP)-tagged D3 (MBP-D3) and
195 Glutathione-S-transferase (GST)-tagged D14L. We found that MBP-D3, but not the control
196 protein MBP-hexahistidine (His), interacted weakly with GST-D14L in the absence of KL
197 analogs. This interaction was enhanced by dMGer, but not by (−)-GR24 (Figure 3A). We then
198 performed pull-down assays using MBP-His-OsSMAX1 and GST-D14L. These proteins
199 interacted even in the absence of KL analogs, and their interaction was also strengthened by

200 the addition of dMGer (Figure 3B). In addition, the pull-down assay using MBP-D3 and GST-
201 OsSMAX1 showed an interaction between these proteins in the absence of KL analogs (Figure
202 3C). These results demonstrate that the components of the KL signaling pathway are capable
203 of directly interacting with one another *in vitro* and that dMGer enhances the interactions of
204 D14L with D3 and OsSMAX1, suggesting its critical role in promoting the assembly of the KL
205 signaling complex.

206

207 **Domains of OsSMAX1 and D53 differentially interact with D14L or D14**

208 As we demonstrated the interaction of D14L and OsSMAX1 and the enhancement of the
209 interaction by dMGer *in vitro*, we next examined the functions of the domains of OsSMAX1.
210 To compare the affinity of the OsSMAX1 D1M and D2 domains to D14L, we pulled down
211 GST-D14 using MBP-His-OsSMAX1-D1M or MBP-His-OsSMAX1-D2. The D1M domain
212 showed a stronger interaction with D14L than the D2 domain. While dMGer enhanced the
213 interaction of the D1M domain with D14L, it did not enhance the interaction of the D2 domain
214 with D14L (Figure 3B). As it has been shown that D3-CTH enhances the interaction between
215 the D53-D2 domain and D14 (Shabek et al., 2018), we examined whether D3-CTH enhances
216 the interaction between the OsSMAX1-D2 domain and D14L. However, D3-CTH did not
217 enhance the interaction between OsSMAX1-D2 domain and D14L either in the absence or
218 presence of dMGer (Figure 3D). We also examined the interaction of the OsSMAX1 domains
219 with D3. The pull-down assay showed an interaction between OsSMAX1-D1M and D3 (Figure
220 3C). These results demonstrate that the OsSMAX1-D1M domain plays a central role in the
221 interaction of OsSMAX1 with D14L and D3.

222 As our results suggested that the functions of OsSMAX1 domains for the interaction with
223 D14L are different from those of D53 domains for the interaction with D14, we investigated
224 the interactions of OsSMAX1 and D53 domains with D14L and D14. In our *in vitro* pull-down
225 assays, D14L strongly interacted with the OsSMAX1-D1M domain, while it hardly interacted
226 with the D53-D1M domain in the presence of dMGer. Although OsSMAX1-D2 and D53-D2
227 domains seem to have similar levels of affinity for D14L, these interactions were much weaker
228 than the interaction between D14L and the OsSMAX1-D1M domain (Figure 4A). In contrast,
229 D14 showed a stronger interaction with the D53-D2 domain in the presence of the D14 ligand
230 (+)-GR24 than with the interactions with D53-D1M, OsSMAX1-D1M, and OsSMAX1-D2

231 domains (Figure 4B). This D14–D53-D2 interaction was enhanced by D3-CTH in a manner
232 consistent with the previous report (Shabek et al., 2018). D3-CTH also increased the interaction
233 efficiency between D14 and the OsSMAX1-D2 domain. The affinities of D14 with the two D2
234 domains in the presence of D3-CTH did not show any apparent difference (Figure 4B). These
235 results suggest that D14–D53 and D14L–OsSMAX1 complexes exhibit distinct binding modes.

236

237 **Discussion**

238 The absence of natural ligands remains a major obstacle to understanding the KL signaling
239 pathway. By using the recently developed artificial KL analog, dMGer, we partially overcome
240 this limitation. We show that dMGer effectively and selectively induces KL responses in rice
241 and directly interacts with D14L. Furthermore, we demonstrate that the direct interaction
242 between D3 and D14L is induced by the ligand. We also report, for the first time, the
243 enhancement of the interaction between D14L/KAI2 and SMAX1 by KL analogs *in vitro*.
244 These findings—obtained without the use of yeast or plant cells—suggest that the three
245 proteins are intrinsically capable of interacting in a KL-responsive manner. Furthermore,
246 parallel comparisons of interactions of D14L and D14 with domains of SMXL and D53
247 revealed regions that contribute to the specificity of KL and SL signaling. Our findings refine
248 our understanding of the molecular basis of the KL signaling pathway.

249 This work is the first report describing the physiological responses of rice to desmethyl-
250 type KL analogs. dMGer has been shown to suppress hypocotyl elongation in a KAI2-
251 dependent manner and to induce seed germination; however, evaluation of its physiological
252 activities has been largely limited to Arabidopsis, except for germination-induction assays with
253 the root parasitic plants *Orobanche minor* and *Striga hermonthica*, in which KAI2-dependency
254 was not examined (Okabe et al., 2023). In the case of other desmethyl-type analogs, their
255 physiological activity has been investigated only in Arabidopsis and *Brachypodium distachyon*
256 (Yao et al., 2021b; Meng et al., 2022). The observed D14L-dependent effects on plant growth
257 and the regulation of KL marker genes demonstrate the function of dMGer as a KL analog in
258 rice, suggesting the potential of desmethyl-type analogs in a wide range of species.

259 In our *in vitro* assays, dMGer and (−)-GR24 exhibited distinct activities. dMGer inhibited
260 dYLG hydrolysis by D14L and induced a Tm shift of D14L in DSF assays, indicating direct

261 binding to the D14L ligand-binding pocket and induction of structural changes in D14L,
262 whereas (−)-GR24 did not induce these responses. Consistently, dMGer, but not (−)-GR24,
263 enhanced the interaction between D14L and D3. The enhancement of the interaction of D14L
264 with D3 or OsSMAX1 by KL analogs *in vitro* has not been reported previously. This may
265 reflect the fact that (−)-GR24, the most commonly used KL analog, shows no activity toward
266 D14L *in vitro*. Similarly, in Arabidopsis, although (−)-GR24 induces a slight Tm shift of KAI2
267 in DSF assay, the shift is much weaker than that induced by dGR24, a desmethyl-type KL
268 analog (Yao et al., 2021b). The enhancement of KAI2-SMAX1 interaction by KL analogs *in*
269 *vitro* has not been reported. Although a report presented the enhancement of KAI2-MAX2
270 interaction by *rac*-GR24 *in vitro*, the interaction is much weaker than the AtD14-MAX2
271 interaction observed under the same conditions (Xu et al., 2018). These results imply that the
272 *in vitro* activity of (−)-GR24 toward KAI2 is insufficient to significantly enhance the
273 interactions of KAI2 with MAX2 and SMAX1. The use of desmethyl-type KL analogs may
274 also reveal the interaction of the KL signaling components in Arabidopsis.

275 Despite the lack of *in vitro* activity of (−)-GR24 toward D14L, it induces KL responses in
276 rice. Several possible explanations could account for the discrepancy between the *in vitro* and
277 *in vivo* activities of (−)-GR24. One explanation is the requirement for *in vivo* conversion of
278 (−)-GR24 into an active molecule, as suggested in the case of KARs. Previous studies
279 demonstrated that neither KAR_1 nor KAR_2 shifts the Tm of KAI2 in DSF assays, and that
280 KAR_1 is slow to induce ubiquitination of SMXL2 (Waters et al., 2015; Wang et al., 2020b).
281 These findings suggest that metabolic processing renders KARs active. (−)-GR24 may likewise
282 undergo metabolic conversion into an unidentified bioactive form *in vivo*. An alternative
283 hypothesis is that KAI2/D14L is subject to post-translational modifications that alter its mode
284 of ligand recognition. Various enzymatic and non-enzymatic post-translational modifications
285 that influence catalytic activity or protein folding have been documented (Kokkinidis et al.,
286 2020). Another possibility is that D14L recognizes (−)-GR24 only in the presence of plant-
287 derived cofactors. As an example of cofactor requirements in plant hormone signaling, binding
288 of inositol pentakisphosphate is essential for CORONATINE INSENSITIVE 1 and JAZ
289 proteins to function as the co-receptor of jasmonate (Sheard et al., 2010).

290 Taking advantage of the *in vitro* activity of dMGer, we characterized the interaction mode
291 of the KL signaling components. In the absence of dMGer, although the interaction between
292 D3 and D14L was hardly detectable, both D3 and D14L interacted with OsSMAX1. dMGer
293 enhanced the interactions of D14L with D3 and OsSMAX1. These results suggest that D14L,

294 D3, and OsSMAX1 form a complex even in the absence of the ligand, and that KL stabilizes
295 and alters the conformation of this ternary complex, thereby leading to ubiquitination of
296 OsSMAX1, although further *in vivo* evaluation is required to confirm this model (Figure 5A).

297 Furthermore, we clarified differences in the mode of interaction between the KL and SL
298 signaling complexes. The selective interaction of D14L with OsSMAX1 relies on its strong
299 affinity to the OsSMAX1-D1M domain rather than the D2 domain. On the other hand, D14
300 prefers the D53-D2 domain rather than the D1M domain. D3-CTH enhances the interaction
301 between D14 and D53-D2, but not the interaction between D14L and OsSMAX1-D2 (Figure
302 5B). These findings demonstrate that although D14 and D14L, as well as D53 and OsSMAX1,
303 are paralogs, they distinctively interact in the KL and SL signaling complexes. Intriguingly,
304 D3-CTH also enhanced the interaction of D14 with OsSMAX1-D2 under our assay conditions.
305 Previously, the *in vivo* interaction between AtD14 and SMAX1/SMXL2 has been reported
306 (Wang et al., 2020b; Li et al., 2022). This interaction may be conserved in rice and mediated
307 by the OsSMAX1-D2 domain and D3-CTH.

308 Our findings are expected to open new avenues for future research in the field of KL
309 signaling. First, dMGer—a potent and readily available artificial KL analog—serves as a
310 powerful experimental tool. In addition to its utility in physiological assays, its ability to
311 efficiently activate the receptor may facilitate structural analyses of KL signaling complexes,
312 which remain unresolved. Furthermore, our study demonstrates that ligand-dependent
313 interaction occurs between D14L and D3. This *in vitro* system could be leveraged for the
314 identification of endogenous KL or for assessing the activity of newly designed KL analogs.
315 Finally, we have identified regions that contribute to the functional divergence between
316 SMAX1 and D53. Further biochemical and structural dissection of these regions may elucidate
317 the molecular basis underlying the divergence of the KL and SL signaling pathways.

318

319 **Materials and Methods**

320 **Plant materials and growth conditions**

321 The rice cultivar Nipponbare was used as the wild type. The *d14l-c1* line was previously
322 described (Mashiguchi et al., 2023). The *d14l-c2* line was generated using the same gRNA as

323 that for *d14l-c1*, as described previously (Mashiguchi et al., 2023). Due to the duplication of
324 the 174th cytosine in the D14L ORF, a frame shift occurs after the 59th amino acid residue,
325 generating a premature stop codon.

326 To test mesocotyl responses to dMGer, rice seeds were surface-sterilized with sodium
327 hypochlorite for 15 minutes and placed on 0.6% (w/v) agarose plates supplemented with the
328 indicated concentrations of the compounds. A 1000× stock solution of dMGer, dissolved in
329 acetone, was added to the medium to achieve the final concentrations. Plates containing 0.1%
330 acetone served as mock controls. Seeds were germinated and grown in the dark at 28 °C for 8
331 days in an incubator. To remove seedlings that did not germinate properly from the analysis,
332 only seedlings that properly developed embryonic roots and had a ≥2-cm of aerial part were
333 measured. Mesocotyl length was measured using Fiji.

334 To test the effects of chemicals on *DLK2b* and *KUF1* transcription, rice seeds were surface-
335 sterilized with sodium hypochlorite for 15 minutes and then grown on solid Hoagland medium
336 containing 0.8% Phytagel for 4 days at 28 °C under a 12-h light/12-h dark cycle. Uniform
337 seedlings were then selected and transferred to 1 mL of Hoagland solution, cultured overnight,
338 and then incubated for 6 hours with 0.1, 1, or 10 μM of (−)-GR24 or dMGer at 28°C. A 1000×
339 stock solution of each compound, dissolved in acetone, was used to achieve the final
340 concentrations. Hoagland solution containing 0.1% (v/v) acetone without any added compound
341 was used as the mock control.

342

343 **qRT-PCR analysis**

344 Total RNA was extracted from rice roots using the EasyPure Plant RNA Kit (TransGen). An
345 aliquot (0.05–0.2 μg) was used for first-strand cDNA synthesis with the TransScript Uni All-
346 in-One First-Strand cDNA Synthesis SuperMix for qPCR (TransGen). RT-qPCR was
347 performed using gene-specific primers (Supplemental Table) on an Agilent Mx3000P system,
348 following the manufacturer's instructions. Each 10 μL reaction contained 1 μL of diluted
349 cDNA, 0.2 μM of each primer, and 5 μL of KOD SYBR qPCR Mix (Toyobo). The rice *UBQ*
350 gene was used as an internal reference.

351

352 **Plasmid construction**

353 To construct the plasmid for expressing His-D14L for DSF assays, the ORF fragment of *D14L*
354 was amplified by PCR from cDNA synthesized from rice total RNA. The PCR product was
355 cloned by In-Fusion (Takarabio) into the pET47b vector (Novagen) using SmaI and SacI sites.
356 To construct the plasmid for expressing MBP-His-D14L, the CDS of *D14L* was amplified from
357 cDNA synthesized from rice total RNA, and the PCR product was inserted into the Sma1 and
358 EcoR1 sites of the modified pMAL-c5x vector (Seto et al., 2019) (pMALHis). For expression
359 of GST-D14L, the *D14L* CDS was subcloned from pMALHis-D14L into pGEX-4T-3 (Cytiva)
360 using EcoRI and NotI sites. For expression of GST-D14, the *D14* (50–318) CDS in cDNA
361 synthesized from rice total RNA was amplified and inserted into pGEX-4T-3 using EcoRI and
362 NotI sites.

363 For the bacterial expression of MBP-His-tagged full-length OsSMAX1 (residues 2–1041)
364 (OsSMAX1-FL) and domains of OsSMAX1 (D1M: 218–541; D2: 638–1041), the
365 corresponding CDS regions were amplified from cDNA synthesized from rice total RNA. PCR
366 products were first inserted into pGEX-4T-3, followed by subcloning into pMALHis, replacing
367 D14L in pMALHis-D14L.

368 For the bacterial expression of MBP-His-tagged domains of D53, the fragments encoding the
369 D1M (182–510) and D2 (718–1131) domains of D53 were amplified from rice genomic DNA.
370 The D53-D1M fragment was produced by overlap extension PCR using two fragments
371 amplified from exon 1 and exon 2 of genomic *D53*. A nonsynonymous substitution found in
372 the amplified D53-D1M fragment was corrected by overlap extension PCR. These fragments
373 were cloned into pMALHis.
374

375 To construct a plasmid for co-expression of MBP-tagged D3 (2–720) and untagged ASK1 in
376 insect cells, the CDSs of *D3* and *ASK1* were amplified from cDNA synthesized from total RNA
377 extracted from rice and Arabidopsis seedlings, respectively. ASK1 was inserted into pFastBac
378 Dual (Thermo Fisher Scientific) at the *Nco*I site downstream of the p10 promoter, yielding
379 pFastBacDual-ASK1. *D3* was first cloned into pGEX-4T-3 and then subcloned into
380 pFastBacDual-ASK1 downstream of the polyhedrin promoter, fused with an MBP tag
381 amplified from pMALHis. For multi-fragment assembly, we used the ClonExpress II One Step
382 Cloning Kit (Vazyme).

383 Primers used for the plasmid construction are listed in Supplemental Table.

384 **Preparation of recombinant proteins**

385 *E. coli* BL21(DE3) was used for the expression of D14L for DSF. The overnight culture (20
386 mL) was added to a fresh LB medium (2.0 L) containing kanamycin (50 mg/L) at 37ºC. After
387 OD600 reached 0.8, 0.25 mM isopropyl β-D-1-thiogalactopyranoside (IPTG) was added, and
388 the culture was further incubated at 18 °C for 21 h. The culture medium was centrifuged at
389 3500 *g* and the pellet was stored at −30ºC until use. The pellet was resuspended and sonicated
390 in lysis buffer (50 mM Tris buffer (pH 8.0) containing 500 mM NaCl, 5 mM 2-
391 mercaptoethanol, and 10 % glycerol). The supernatant was purified using His60 Ni
392 Superflow Resin (1 mL, Takara). After washing with the washing buffer (50 mM Tris buffer
393 (pH 8.0) containing 500 mM NaCl and 20 mM imidazole), the bound protein was eluted with
394 elution buffer (50 mM Tris buffer (pH 8.0) containing 500 mM NaCl and 200 mM
395 imidazole). The eluate was concentrated using VIVASPIN Turbo 15 (Sartorius), adjusted to
396 12 mg/mL, aliquoted, immediately frozen in liquid nitrogen, and stored at −80ºC until use.

397 *E.coli* strain Rosetta (DE3) (Novagen) was used for the production of recombinant proteins,
398 except for D3 and ASK1, for *in vitro* pull-down assays and dYLG assays. Transformed cells
399 were cultured in LB media containing 50 µg/mL carbenicillin and 50 µg/mL chloramphenicol
400 at 16 °C until the OD_{600} reached 0.4–0.6. Protein expression was induced with 0.1 mM IPTG,
401 and cells were incubated overnight at 16 °C.

402 For purification of MBP-6×His-fused D14L, OsSMAX1-D1M, OsSMAX1-D2, OsSMAX1-
403 FL, D53-D1M, D53-D2, and the MBP-6×His control protein, cells were harvested by
404 centrifugation and lysed by sonication in lysis buffer (25 mM Tris-HCl, pH 8.0, 500 mM NaCl,
405 1 mM TCEP, 20 mM imidazole, and 0.4 mM phenylmethylsulfonyl fluoride (PMSF)). The
406 lysate was centrifuged at 18,000 rpm for 50 min at 4 °C. The supernatant was applied to Ni
407 NTA Beads (Smart-Lifesciences) in a Poly-Prep Chromatography Column (Bio-Rad). After
408 washing with lysis buffer, proteins were eluted with MBP elution buffer (20 mM Tris-HCl,
409 pH 8.0, 500 mM NaCl, 1 mM TCEP, and 250 mM imidazole). The eluate was subsequently
410 applied to Dextrin Beads (Smart-Lifesciences) in a Poly-Prep Chromatography Column. After
411 washing with MBP wash buffer (20 mM Tris-HCl, pH 8.0, 500 mM NaCl, 1 mM TCEP),
412 proteins were eluted with MBP elution buffer (MBP wash buffer containing 10 mM maltose).
413 Eluted proteins were concentrated and subjected to buffer exchange using Amicon Ultra-15

414 (10 kDa MWCO for MBP-6×His, 30 kDa for the others). The buffer was exchanged first to
415 MBP wash buffer, and then to either 100 mM Tris-HCl, pH 7.6, 150 mM NaCl, 0.5 mM TCEP
416 (for D14L), 20 mM Tris-HCl, pH 7.5, 500 mM NaCl, 0.5 mM TCEP (for OsSMAX1-D1M,
417 and D53-D1M), 50 mM Tris-HCl, pH 7.5, 500 mM NaCl, 0.5 mM TCEP (for OsSMAX1-D2
418 and D53-D2), or 20 mM Tris, pH 8.0, 500 mM NaCl, 0.5 mM TCEP (for OsSMAX1-FL, MBP-
419 6xHis). In the final dialyzed samples, the residual concentrations of MBP elution and MBP
420 wash buffers were less than 0.2% and 1% (v/v), respectively.

421 For purification of GST-D14L and GST-D14, cells were harvested by centrifugation and lysed
422 by sonication in lysis buffer (25 mM Tris-HCl, pH 7.6, 500 mM NaCl, 1 mM TCEP, and
423 0.4 mM PMSF). The lysate was centrifuged at 18,000 rpm for 50 min at 4 °C. The supernatant
424 was applied to Glutathione Beads (Smart-Lifesciences) packed in a Poly-Prep Chromatography
425 Column. After sequential washing with lysis buffer and GST wash buffer (100 mM Tris-HCl,
426 pH 8.0, 500 mM NaCl, 1 mM TCEP), proteins were eluted with GST elution buffer (100 mM
427 Tris-HCl, pH 8.0, 500 mM NaCl, and 20 mM reduced glutathione). Eluted proteins were
428 concentrated and subjected to buffer exchange using Amicon Ultra-15 centrifugal filters
429 (30 kDa MWCO). The buffer was first exchanged to dialysis buffer 1 (100 mM Tris-HCl,
430 pH 8.0, 500 mM NaCl, 0.5 mM TCEP), and then to 50 mM Tris-HCl, pH 7.5, 150 mM NaCl,
431 0.5 mM TCEP. In the final dialyzed samples, the residual concentrations of GST elution and
432 dialysis buffer 1 were less than 0.2% and 1% (v/v), respectively.

433 For purification of GST-fused OsSMAX1-D1M, OsSMAX1-D2, and OsSMAX1-FL, the same
434 lysis, GST wash, and GST elution buffers as those for the purification of GST-D14L and GST-
435 D14 were used. For OsSMAX1-D1M and OsSMAX1-FL, the sonicated cell lysate was mixed
436 with polyethylenimine (Sinopharm Chemical Reagent Co., Ltd) to a final concentration of
437 approximately 0.1%(w/v) before centrifugation at 18,000 rpm. Subsequent purification with
438 Glutathione Beads was similar to that for GST-D14L/D14. Eluted proteins were concentrated
439 and subjected to buffer exchange using Amicon Ultra-15 centrifugal filters (30 kDa MWCO).
440 The buffer was first exchanged to dialysis buffer 1, and then to either 50 mM HEPES-NaOH,
441 pH 7.0, 500 mM NaCl, 0.5 mM TCEP (for D1M and FL) or 50 mM HEPES-NaOH, pH 7.0,
442 500 mM NaCl, 1 mM TCEP (for D2).

443 MBP-tagged D3 was co-expressed with untagged ASK1 in *Spodoptera frugiperda* Sf9 cells.
444 Suspension cultures were infected with recombinant baculovirus generated using the Bac-to-

445 Bac Baculovirus Expression System (Thermo Fisher Scientific), following the manufacturer's
446 instructions. Cells were harvested by centrifugation and lysed by sonication in 50 mM Tris-
447 HCl, pH 7.5, 200 mM NaCl, 0.5 mM TCEP, 1% Protease Inhibitor Cocktail (EDTA-Free)
448 (APExBIO, K1007). The lysate was clarified by centrifugation at 18,000 rpm for 50 min at
449 4 °C, and the supernatant was applied to Dextrin Beads (Smart Lifesciences) in a Poly-Prep
450 chromatography column (Bio-Rad). After washing with D3 wash buffer (50 mM Tris-HCl,
451 pH 7.5, 200 mM NaCl, 0.5 mM TCEP), bound proteins were eluted with D3 elution buffer (D3
452 wash buffer supplemented with 10 mM maltose). Eluted proteins were concentrated and
453 subjected to buffer exchange using Amicon Ultra-4 (10 kDa MWCO). The buffer was first
454 exchanged to D3 wash buffer, followed by 50 mM Tris-HCl, pH 7.5, 150 mM NaCl, 0.5 mM
455 TCEP. In the final dialyzed samples, the residual concentrations of D3 elution and D3 wash
456 buffers were less than 0.1% and 1% (v/v), respectively.

457

458 **Differential scanning fluorometry experiments**

459 DSF was conducted using 4.8 μg of the recombinant D14L protein in 20 μL of PBS buffer
460 containing the 0.005 μL of Sypro Orange (Ex/Em: 490/610 nm; Invitrogen) and the tested
461 compound with 5% (v/v) acetone on a 96-well plate. Mixtures were heated from 20ºC to 95ºC,
462 and the fluorescence (Ex/Em; 490/610) was continuously scanned by using LightCycler480.
463 The denaturation curve was calculated by using the LightCycler480 Software.

464

465 **dYLG hydrolysis assays**

466 Reactions contained 1 μM dYLG, 0–5 μM competitor, 0.3% DMSO, and 10 μg/mL MBP-
467 6×His-D14L. Recombinant protein (10 mg/mL in 100 mM Tris-HCl, pH 7.6, 150 mM NaCl,
468 0.5 mM TCEP) was diluted 500-fold with reaction buffer (100 mM HEPES, pH 7.0, 150 mM
469 NaCl). dYLG (1 mM stock in DMSO) and the competitor (500× stock in DMSO) were diluted
470 with reaction buffer to twice their final concentrations before addition to the reaction. Protein
471 solution (25 μL/well) was dispensed into a 1/2 Area OptiPlate-96 (PerkinElmer), followed by
472 the addition of an equal volume of the dYLG/competitor solution, on ice. Fluorescence
473 intensity was measured at 30 °C in the dark (Ex/Et: 480/520 nm) using Varioskan Flash
474 (Thermo Fisher Scientific).

475

476 **Pull-down assays**

477 The of D14L with D3 or domains of OsSMAX1/D53 were assessed using 2.5 μg GST-D14L
478 (prey protein) was incubated with an approximately equimolar MBP-His (as a control) or
479 MBP-tagged bait proteins at 4 °C in 700 μL of incubation buffer (20 mM Bis-Tris-HCl,
480 pH 7.0, 150 mM NaCl, 0.1% Triton X-100, 0.2% DMSO for D3; 20 mM Tris-HCl, pH 7.5,
481 150 mM NaCl, 0.1% Triton X-100, 0.2% DMSO for the others). After ~1 h of incubation,
482 25 μL of 50% Dextrin Beads (Smart Lifesciences) slurry, equilibrated and suspended in
483 incubation buffer without KL analog, were added and incubated at 4 °C for ~1.5 h. Beads
484 were washed three times with incubation buffer, and bound proteins were eluted with elution
485 buffer (20 mM Bis-Tris-HCl, pH 7.0, 150 mM NaCl, 10 mM maltose for D3; 20 mM Tris-
486 HCl, pH 7.5, 150 mM NaCl, 10 mM maltose for the others). Eluates were mixed with an
487 equal volume of 2× SDS-PAGE sample buffer and boiled at 95 °C for 5 min. To test the
488 effects of dMGer or (−)-GR24, 10 μM of each chemical was added to the incubation buffer.
489 When testing the effects of D3-CTH, synthesized D3-CTH peptideswere added at an
490 approximately equimolar to the prey protein, and the beads were washed with incubation
491 buffer containing no peptide.

492 The interactions of D14 with domains of OsSMAX1/D53 were assessed using similar
493 procedures to those for D14L. 10 μM (+)-GR24 was added to the incubation buffer (20 mM
494 Tris-HCl, pH 7.5, 150 mM NaCl, 0.1% Triton X-100, 0.2% DMSO).

495 To assess the interactions between D3 and domains of OsSMAX1, 5 μg of MBP-D3-ASK1
496 and 2 μg of MBP-6×His (control) were incubated with an approximately equimolar amounts
497 of GST-tagged bait proteins or GST (control) in 700 μL of incubation buffer (20 mM Tris-HCl,
498 pH 7.5, 150 mM NaCl, 0.5 mM TCEP, 0.1% Triton X-100). After ~1 h of incubation, 25 μL of
499 50% Glutathione Beads (Smart Lifesciences) slurry, equilibrated and suspended in incubation
500 buffer, was added and incubated at 4 °C for ~1.5 h. Beads were washed three times with
501 incubation buffer, and bound proteins were eluted with elution buffer (100 mM Tris-HCl,
502 pH8.0, 150 mM NaCl, 20 mM Reduced glutathione). Eluates were mixed with an equal volume
503 of 2× SDS-PAGE sample buffer and boiled at 95 °C for 5 min.

504 Input and eluted proteins were resolved by SDS-PAGE and detected by western blotting.
505 Western blots were performed using mouse anti-GST antibody (Beijing Protein Innovation,
506 AbM59001-2H5-PU; 1:3000–1:1000 diluted), mouse anti-MBP antibody (Beijing Protein

507 Innovation, AbM59007-3-PU; 1:6000–1:1000 diluted), and HRP-conjugated goat anti-mouse
508 IgG (H+L) (ABclonal, AS003; 1:10000 diluted).

509

510 **Funding**
511 This research was supported by the Key Laboratory of Plant Carbon Capture, Chinese
512 Academy of Sciences.

513

514 **Author contributions**

515 H.K. and K.T. designed the research. K.T. performed the mesocotyl elongation, dYLG, and
516 pull-down assays. J.W. performed the gene expression analysis. Y.H., T.S., and Y.S. performed
517 the DSF assay. Y.Y. contributed to plasmid construction and protein purification. H.K. assisted
518 in data analysis. K.T. and H.K. wrote the manuscript.

519

520 **Acknowledgements**
521 We thank to Miaolian Ma (Eukaryotic Protein Expression and Purification Platform, CAS
522 CEMPS) for technical support in protein expression using insect cell culture, Liu Li (Core
523 Facility Center of CEMPS, CAS) for technical instruction on fluorescence measurements, Prof.
524 Dr. Minrui Fan (CAS CEMPS) for access to the equipment for protein extraction, Prof. Dr.
525 Ruiqiang Ye (CAS CEMPS) for access to the equipment for western blot, and Dr. Kosuke Fukui
526 (Tokyo University of Science) for providing dMGer.

527

528 **Declaration of interests**

529 The authors declare no competing interests.

530

531

532

References

Abe, S., Sado, A., Tanaka, K., Kisugi, T., Asami, K., Ota, S., Kim, H. I., Yoneyama, K., Xie, X., Ohnishi, T., et al. (2014). Carlactone is converted to carlactonoic acid by MAX1 in *Arabidopsis* and its methyl ester can directly interact with AtD14 in vitro. *Proc. Natl Acad. Sci. U.S.A.* **111**:18084–18089.

Carbonnel, S., Das, D., Varshney, K., Kolodziej, M. C., Villaécija-Aguilar, J. A., and Gutjahr, C. (2020). The karrikin signaling regulator SMAX1 controls *Lotus japonicus* root and root hair development by suppressing ethylene biosynthesis. *Proc. Natl Acad. Sci. U.S.A.* **117**:21757–21765.

Chiwocha, S. D. S., Dixon, K. W., Flematti, G. R., Ghisalberti, E. L., Merritt, D. J., Nelson, D. C., Riseborough, J.-A. M., Smith, S. M., and Stevens, J. C. (2009). Karrikins: A new family of plant growth regulators in smoke. *Plant Science* **177**:252–256.

Choi, J., Lee, T., Cho, J., Servante, E. K., Pucker, B., Summers, W., Bowden, S., Rahimi, M., An, K., An, G., et al. (2020). The negative regulator SMAX1 controls mycorrhizal symbiosis and strigolactone biosynthesis in rice. *Nat. Commun.* **11**:2114. https://doi.org/10.1038/s41467-020-16021-1

Conn, C. E., and Nelson, D. C. (2016). Evidence that KARRIKIN-INSENSITIVE2 (KAI2) Receptors may Perceive an Unknown Signal that is not Karrikin or Strigolactone. *Front. Plant Sci.* **6**. https://doi.org/10.3389/fpls.2015.01219.

de Saint Germain, A., Clavé, G., Badet-Denisot, M.-A., Pillot, J.-P., Cornu, D., Le Caer, J.-P., Burger, M., Pelissier, F., Retailleau, P., Turnbull, C., et al. (2016). An histidine covalent receptor and butenolide complex mediates strigolactone perception. *Nat. Chem. Biol.* **12**:787–794.

Fukui, K., Arai, K., Kasahara, H., Asami, T., and Hayashi, K. (2019). Synthetic agonist of HTL/KAI2 shows potent stimulating activity for *Arabidopsis* seed germination. *Bioorg. Med. Chem. Lett.* **29**:2487–2492.

Gutjahr, C., Gobbato, E., Choi, J., Riemann, M., Johnston, M. G., Summers, W., Carbonnel, S., Mansfield, C., Yang, S.-Y., Nadal, M., et al. (2015). Rice perception of symbiotic arbuscular mycorrhizal fungi requires the karrikin receptor complex. *Science* **350**:1521–1524.

Hamiaux, C., Drummond, R. S. M., Janssen, B. J., Ledger, S. E., Cooney, J. M., Newcomb, R. D., and Snowden, K. C. (2012). DAD2 Is an α/β Hydrolase Likely to Be Involved in the Perception of the Plant Branching Hormone, Strigolactone. *Current Biology* **22**:2032–2036.

Jiang, L., Liu, X., Xiong, G., Liu, H., Chen, F., Wang, L., Meng, X., Liu, G., Yu, H., Yuan, Y., et al. (2013). DWARF 53 acts as a repressor of strigolactone signalling in rice. *Nature* **504**:401–405.

Kameoka, H., and Kyozuka, J. (2015). Downregulation of Rice *DWARF 14 LIKE* Suppress Mesocotyl Elongation *via* a Strigolactone Independent Pathway in the Dark. *J. Genet. Genomics* **42**:119–124.

Khosla, A., Morffy, N., Li, Q., Faure, L., Chang, S. H., Yao, J., Zheng, J., Cai, M. L., Stanga, J., Flematti, G. R., et al. (2020). Structure–Function Analysis of SMAX1 Reveals Domains That Mediate Its Karrikin-Induced Proteolysis and Interaction with the Receptor KAI2. *Plant Cell* **32**:2639–2659.

Kokkinidis, M., Glykos, N. M., and Fadouloglou, V. E. (2020). Catalytic activity regulation through post-translational modification: the expanding universe of protein diversity. *Adv. Protein Chem. Struct. Biol* **122**:97–125.

Kushihara, R., Nakamura, A., Takegami, K., Seto, Y., Kato, Y., Dohra, H., Ohnishi, T., Todoroki, Y., and Takeuchi, J. (2025). Structural requirements of KAI2 ligands for activation of signal transduction. *Proc. Natl Acad. Sci. U.S.A.* **122**:e2414779122. https://doi.org/10.1073/pnas.2414779122.

Li, W., Nguyen, K. H., Chu, H. D., Ha, C. V., Watanabe, Y., Osakabe, Y., Leyva-González, M. A., Sato, M., Toyooka, K., Voges, L., et al. (2017). The karrikin receptor KAI2 promotes drought resistance in Arabidopsis thaliana. *PLOS Genetics* **13**:e1007076. https://doi.org/10.1371/journal.pgen.1007076

Li, Q., Martín-Fontecha, E. S., Khosla, A., White, A. R. F., Chang, S., Cubas, P., and Nelson, D. C. (2022). The strigolactone receptor D14 targets SMAX1 for degradation in response to GR24 treatment and osmotic stress. *Plant Commun.* **3**:100303. https://doi.org/10.1016/j.xplc.2022.100303

Mashiguchi, K., Morita, R., Tanaka, K., Kodama, K., Kameoka, H., Kyozuka, J., Seto, Y., and Yamaguchi, S. (2023). Activation of Strigolactone Biosynthesis by the DWARF14-LIKE/KARRIKIN-INSENSITIVE2 Pathway in Mycorrhizal Angiosperms, but Not in Arabidopsis, a Non-mycorrhizal Plant. *Plant and Cell Physiol.* **64**:1066–1078.

Meng, Y., Varshney, K., Incze, N., Badics, E., Kamran, M., Davies, S. F., Oppermann, L. M. F., Magne, K., Dalmais, M., Bendahmane, A., et al. (2022). *KARRIKIN INSENSITIVE2* regulates leaf development, root system architecture and arbuscular-mycorrhizal symbiosis in *Brachypodium distachyon*. *Plant J.* **109**:1559–1574.

Mizuno, Y., Komatsu, A., Shimazaki, S., Naramoto, S., Inoue, K., Xie, X., Ishizaki, K., Kohchi, T., and Kyozuka, J. (2021). Major components of the KARRIKIN INSENSITIVE2-dependent signaling pathway are conserved in the liverwort Marchantia polymorpha. *Plant Cell* **33**:2395–2411.

Niesen, F. H., Berglund, H., and Vedadi, M. (2007). The use of differential scanning fluorimetry to detect ligand interactions that promote protein stability. *Nat. Protoc.* **2**:2212–2221.

Okabe, S., Kitaoka, K., Suzuki, T., Kuruma, M., Hagihara, S., Yamaguchi, S., Fukui, K., and Seto, Y. (2023). Desmethyl type germinone, a specific agonist for the HTL/KAI2

receptor, induces the Arabidopsis seed germination in a gibberellin-independent manner. *Biochem. Biophys. Res. Commun.* **649**:110–117.

Sepulveda, C., Guzmán, M. A., Li, Q., Villaécija-Aguilar, J. A., Martinez, S. E., Kamran, M., Khosla, A., Liu, W., Gendron, J. M., Gutjahr, C., et al. (2022). KARRIKIN UP-REGULATED F-BOX 1 (KUF1) imposes negative feedback regulation of karrikin and KAI2 ligand metabolism in Arabidopsis thaliana. *Proc. Natl Acad. Sci. U.S.A.* **119**:e2112820119. https://doi.org/10.1073/pnas.2112820119

Seto, Y., Yasui, R., Kameoka, H., Tamiru, M., Cao, M., Terauchi, R., Sakurada, A., Hirano, R., Kisugi, T., Hanada, A., et al. (2019). Strigolactone perception and deactivation by a hydrolase receptor DWARF14. *Nat. Commun.* **10**:191. https://doi.org/10.1038/s41467-018-08124-7

Shabek, N., Ticchiarelli, F., Mao, H., Hinds, T. R., Leyser, O., and Zheng, N. (2018). Structural plasticity of D3–D14 ubiquitin ligase in strigolactone signalling. *Nature* **563**:652–656.

Sheard, L. B., Tan, X., Mao, H., Withers, J., Ben-Nissan, G., Hinds, T. R., Kobayashi, Y., Hsu, F.-F., Sharon, M., Browse, J., et al. (2010). Jasmonate perception by inositol-phosphate-potentiated COI1–JAZ co-receptor. *Nature* **468**:400–405.

Soundappan, I., Bennett, T., Morffy, N., Liang, Y., Stanga, J. P., Abbas, A., Leyser, O., and Nelson, D. C. (2015). SMAX1-LIKE/D53 Family Members Enable Distinct MAX2-Dependent Responses to Strigolactones and Karrikins in Arabidopsis. *Plant Cell* **27**:3143–59

Tal, L., Guercio, A. M., Varshney, K., Young, A., Gutjahr, C., and Shabek, N. (2023). C-terminal conformational changes in SCF-D3/MAX2 ubiquitin ligase are required for KAI2-mediated signaling. *New Phytol.* **239**:2067–2075.

Villaécija-Aguilar, J. A., Hamon-Josse, M., Carbonnel, S., Kretschmar, A., Schmidt, C., Dawid, C., Bennett, T., and Gutjahr, C. (2019). SMAX1/SMXL2 regulate root and root hair development downstream of KAI2-mediated signalling in Arabidopsis. *PLOS Genet.* **15**:e1008327. https://doi.org/10.1371/journal.pgen.1008327

Wang, L., Wang, B., Jiang, L., Liu, X., Li, X., Lu, Z., Meng, X., Wang, Y., Smith, S. M., and Li, J. (2015). Strigolactone Signaling in Arabidopsis Regulates Shoot Development by Targeting D53-Like SMXL Repressor Proteins for Ubiquitination and Degradation. *Plant Cell* **27**:3128–3142.

Wang, L., Wang, B., Yu, H., Guo, H., Lin, T., Kou, L., Wang, A., Shao, N., Ma, H., Xiong, G., et al. (2020a). Transcriptional regulation of strigolactone signalling in Arabidopsis. *Nature* **583**:277–281.

Wang, L., Xu, Q., Yu, H., Ma, H., Li, X., Yang, J., Chu, J., Xie, Q., Wang, Y., Smith, S. M., et al. (2020b). Strigolactone and Karrikin Signaling Pathways Elicit Ubiquitination and Proteolysis of SMXL2 to Regulate Hypocotyl Elongation in Arabidopsis. *The Plant Cell* **32**:2251–2270.

Waters, M. T., Nelson, D. C., Scaffidi, A., Flematti, G. R., Sun, Y. K., Dixon, K. W., and Smith, S. M. (2012a). Specialisation within the DWARF14 protein family confers distinct responses to karrikins and strigolactones in Arabidopsis. *Development* **139**:1285–1295.

Waters, M. T., Nelson, D. C., Scaffidi, A., Flematti, G. R., Sun, Y. K., Dixon, K. W., and Smith, S. M. (2012b). Specialisation within the DWARF14 protein family confers distinct responses to karrikins and strigolactones in *Arabidopsis*. *Development* **139**:1285–1295.

Waters, M. T., Scaffidi, A., Moulin, S. L. Y., Sun, Y. K., Flematti, G. R., and Smith, S. M. (2015). A Selaginella moellendorffii Ortholog of KARRIKIN INSENSITIVE2 Functions in Arabidopsis Development but Cannot Mediate Responses to Karrikins or Strigolactones. *The Plant Cell* **27**:1925–1944.

Xu, Y., Miyakawa, T., Nosaki, S., Nakamura, A., Lyu, Y., Nakamura, H., Ohto, U., Ishida, H., Shimizu, T., Asami, T., et al. (2018). Structural analysis of HTL and D14 proteins reveals the basis for ligand selectivity in Striga. *Nat Commun* **9**:3947. https://doi.org/10.1038/s41467-018-06452-2

Yao, J., Mashiguchi, K., Scaffidi, A., Akatsu, T., Melville, K. T., Morita, R., Morimoto, Y., Smith, S. M., Seto, Y., Flematti, G. R., et al. (2018). An allelic series at the *KARRIKIN INSENSITIVE 2* locus of *Arabidopsis thaliana* decouples ligand hydrolysis and receptor degradation from downstream signalling. *Plant J.* **96**:75–89.

Yao, J., Scaffidi, A., Meng, Y., Melville, K. T., Komatsu, A., Khosla, A., Nelson, D. C., Kyozuka, J., Flematti, G. R., and Waters, M. T. (2021a). Desmethyl butenolides are optimal ligands for karrikin receptor proteins. *New Phytol.* **230**:1003–1016.

Yao, J., Scaffidi, A., Meng, Y., Melville, K. T., Komatsu, A., Khosla, A., Nelson, D. C., Kyozuka, J., Flematti, G. R., and Waters, M. T. (2021b). Desmethyl butenolides are optimal ligands for karrikin receptor proteins. *New Phytol.* **230**:1003–1016.

Zheng, J., Hong, K., Zeng, L., Wang, L., Kang, S., Qu, M., Dai, J., Zou, L., Zhu, L., Tang, Z., et al. (2020). Karrikin Signaling Acts Parallel to and Additively with Strigolactone Signaling to Regulate Rice Mesocotyl Elongation in Darkness. *Plant Cell* **32**:2780–2805.

Zhou, F., Lin, Q., Zhu, L., Ren, Y., Zhou, K., Shabek, N., Wu, F., Mao, H., Dong, W., Gan, L., et al. (2013). D14–SCFD3-dependent degradation of D53 regulates strigolactone signalling. *Nature* **504**:406–410.

685 **Figure legends**

686

687 **Figure 1. Response of rice seedlings to (−)-GR24 and desmethyl germinone treatments.**

688 (**A**) Representative images of 8-day-old wild-type (WT) and *d14l-c2* seedlings treated with 1
689 μM desmethyl germinone (dMGer) or 0.1% (v/v) acetone as a control. Scale bars: 1 cm.

690 (**B**) Length of mesocotyls of WT and *d14l-c2* plants treated with or without dMGer. Circles
691 represent individual data points. Open squares indicate means of each treatment group. Sample
692 numbers are presented above the plot for each condition. For statistical analysis, Welch's t-test
693 with Bonferroni correction was performed comparing the control and dMGer-treated groups of
694 each genotype. Calculated *p*-values are presented above the plots for each genotype.

695 (**C**, **D**) Transcript levels of *DLK2b* (**C**) and *KUF1* (**D**) in 5-day-old WT rice roots treated with
696 varying concentrations of (−)-GR24 or dMGer, or with 0.1% (v/v) acetone as control (n = 3).
697 Values are expressed as fold change relative to the mean value of the control. Circles represent
698 individual data points; bars indicate means of triplicates. Different letters denote statistically
699 significant differences according to Tukey's HSD test.

700 (**E**, **F**) Transcript levels of *DLK2b* (**E**) and *KUF1* (**F**) in 5-day-old WT and *d14l-c1* mutant
701 roots treated with 10 μM (−)-GR24 or dMGer (n = 3). Acetone (0.1% (v/v)) was used as the
702 control treatment. Values are expressed relative to the mean value of the control WT plants.
703 Circles represent individual data points; bars indicate means of triplicates. Different letters
704 denote statistically significant differences according to Tukey's HSD test.

705

706 **Figure 2. Binding of (−)-GR24 and desmethyl germinone to D14L *in vitro*.**

707 (**A**) Differential scanning fluorimetry (DSF) of MBP-His-D14L in the presence of 0–100 μM
708 (−)-GR24 (left) or desmethyl germinone (dMGer) (right). Melting curves of the protein
709 incubated with the indicated concentrations of each compound are shown in different colors.
710 Each line represents a single replicate (triplicates for each concentration). Control experiments,
711 in which the protein was incubated without KL analogs, are shown in both plots.

712 (**B**) Inhibitory effects of dMGer and (−)-GR24 on dYLG hydrolysis by MBP-6×His-D14L.
713 Reactions contained 1 μM dYLG, 10 ng/μL protein, and the indicated concentrations of (−)-

714 GR24 or dMGer. Dimethyl sulfoxide without either compound served as the mock control.
715 Circles represent individual data points, expressed relative to the mean fluorescence intensity
716 of mock reactions; bars indicate means (n = 4).

717

718 **Figure 3. Interactions between KL-signaling components.**

719 (**A**) *In vitro* MBP pull-down assay using dextrin agarose beads, with MBP-D3 co-expressed
720 with ASK1 or MBP-His tag alone as bait, and GST-D14L as prey. All reactions contained 0.2%
721 (v/v) DMSO as solvent for chemicals. Assays were supplemented with either 10 μM dMGer,
722 10 μM (−)-GR24, or DMSO only. Calculated molecular masses: GST-D14L, ~56 kDa; MBP-
723 D3, ~121 kDa; MBP-His tag, ~45 kDa.

724 (**B**) *In vitro* MBP pull-down assay using MBP-His-tagged full-length (FL) or domain fragments
725 of OsSMAX1 as bait, and GST-D14L as prey. Assays were performed with or without 10 μM
726 dMGer. For better visualization of GST-D14L pulled-down by each bait, images of the same
727 blot taken with different exposure times (short and long) are shown. Calculated molecular
728 masses: MBP-His-OsSMAX1 FL, ~154 kDa; MBP-His-OsSMAX1-D1M, ~79 kDa; MBP-
729 His-OsSMAX1-D2, ~90 kDa.

730 (**C**) *In vitro* GST pull-down assay using glutathione agarose beads, with GST-tagged FL or
731 domains of OsSMAX1 as bait, and MBP-D3 or MBP-His as prey. Calculated molecular
732 masses: GST-OsSMAX1 FL, ~135 kDa; GST-OsSMAX1-D1M, ~60 kDa; GST-OsSMAX1-
733 D2, ~71 kDa; GST tag, ~28 kDa.

734 (**D**) *In vitro* MBP pull-down assay using MBP-His-OsSMAX1-D2 as bait and GST-D14L as
735 prey, performed in the presence or absence of D3-CTH peptide, with or without 10 μM dMGer.

736 GST- and MBP(-His)-tagged proteins were detected by immunoblotting with anti-GST and
737 anti-MBP antibodies, respectively. The positions of size markers electrophoresed with the
738 samples are shown alongside each blot.

739

740 **Figure 4. Differential interaction of D14L and D14 with domains of OsSMAX1 and D53.**
741 (**A**) *In vitro* MBP pull-down assay using MBP-His-tagged domains of D53 or OsSMAX1 as
742 bait, and GST-D14L as prey. All reactions contained 10 μM dMGer. Calculated molecular
743 masses: MBP-His-D53-D1M, ~80 kDa; MBP-His-D53-D2, ~91 kDa.

744 (**B**) *In vitro* MBP pull-down assay using MBP-His-tagged domains of D53 or OsSMAX1 as
745 bait, and GST-D14 as prey, performed in the presence or absence of D3-CTH. All reactions
746 contained 10 μM (+)-GR24. Calculated molecular masses: GST-D14 ~56 kDa.

747 GST- and MBP-His-tagged proteins were detected by immunoblotting with anti-GST and anti-
748 MBP antibodies, respectively. The positions of size markers electrophoresed with the samples
749 are shown alongside each blot.

750

751 **Figure 5. Interactions between rice KL-signaling components and effects of KL.**

752 (**A**) Model of KL-triggered changes in protein–protein interactions. Even in the absence of KL,
753 OsSMAX1 interacts with both D14L and D3, potentially forming a single complex. KL
754 promotes direct binding between D14L and D3 and enhances the interaction between D14L
755 and OsSMAX1, likely stabilizing and altering the conformation of the complex, thereby
756 leading to the ubiquitination of OsSMAX1. Differences in interaction strength are indicated by
757 the thickness of grey lines.

758 (**B**) Schematic of physical interactions of rice D14L and D14 with domains of OsSMAX1 and
759 D53. D14L mainly interacts with OsSMAX1-D1M, whereas D14 mainly interacts with D53-
760 D2. D3-CTH enhances the interaction between D14 and the D53-D2 domain. Differences in
761 interaction strength are indicated by the thickness of grey lines.

762

763 **Supplemental information**

764 **Supplemental Figure 1. Structure of compounds used in this study.**

765 Chemical structures of desmethyl germinone (dMGer) (top left), desmethyl Yoshimulactone
766 Green (dYLG) (top right), (−)-GR24 (bottom left), and (+)-GR24 (bottom right).

767

768 **Supplemental Figure 2. Uncropped blots.**

769 (**A**) Full western blot images of Figure 3A.
770 (**B**) Full western blot images of Figure 3B.
771 (**C**) Full western blot images of Figure 3C.
772 (**D**) Full western blot images of Figure 3D.
773 (**E**) Full western blot images of Figure 4A.
774 (**F**) Full western blot images of Figure 4B.

775

776 **Supplemental Table. List of primers used in this study.**

777

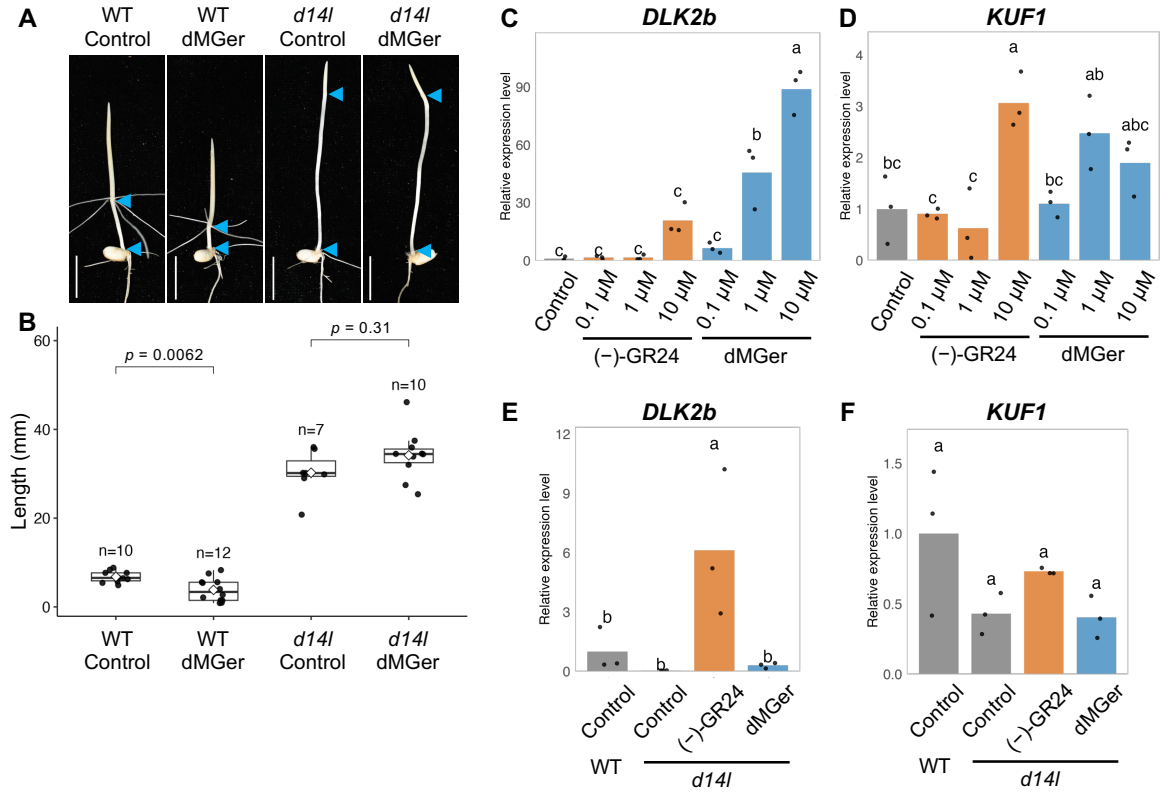

Figure 1. Response of rice seedlings to (−)-GR24 and desmethyl germinone treatments.

(**A**) Representative images of 8-day-old wild-type (WT) and *d14l-c2* seedlings treated with 1 μM desmethyl germinone (dMGer) or 0.1% (v/v) acetone as a control. Scale bars: 1 cm.

(**B**) Length of mesocotyls of WT and *d14l-c2* plants treated with or without dMGer. Circles represent individual data points. Open squares indicate means of each treatment group. Sample numbers are presented above the plot for each condition. For statistical analysis, Welch's t-test with Bonferroni correction was performed comparing the control and dMGer-treated groups of each genotype. Calculated *p*-values are presented above the plots for each genotype.

(**C**, **D**) Transcript levels of *DLK2b* (**C**) and *KUF1* (**D**) in 5-day-old WT rice roots treated with varying concentrations of (−)-GR24 or dMGer, or with 0.1% (v/v) acetone as control (n = 3). Values are expressed as fold change relative to the mean value of the control. Circles represent individual data points; bars indicate means of triplicates. Different letters denote statistically significant differences according to Tukey's HSD test.

(**E**, **F**) Transcript levels of *DLK2b* (**E**) and *KUF1* (**F**) in 5-day-old WT and *d14l-c1* mutant roots treated with 10 μM (−)-GR24 or dMGer (n = 3). Acetone (0.1% (v/v)) was used as the

control treatment. Values are expressed relative to the mean value of the control WT plants. Circles represent individual data points; bars indicate means of triplicates. Different letters denote statistically significant differences according to Tukey's HSD test.

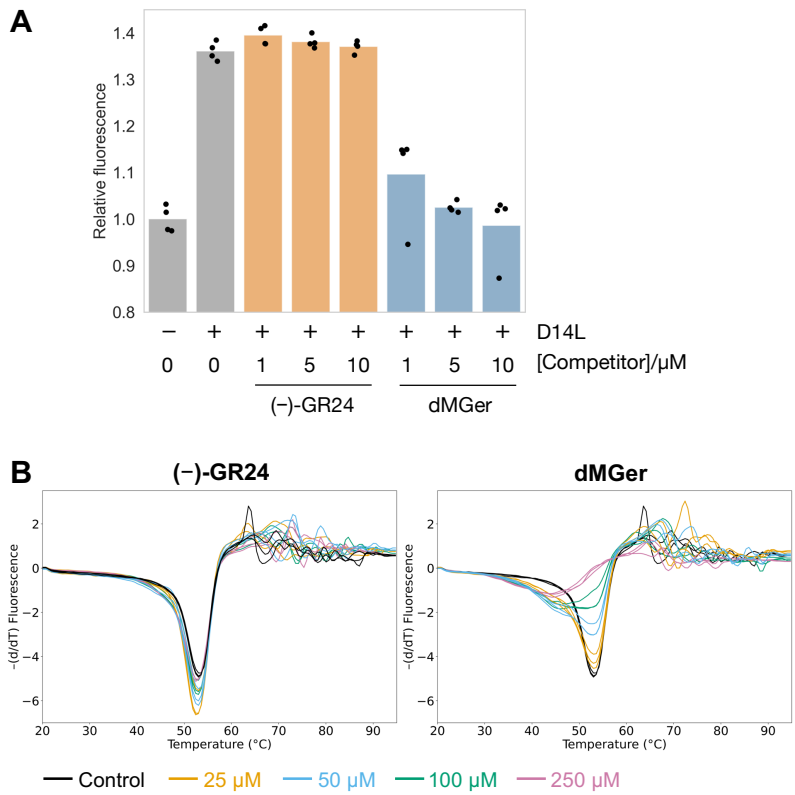

Figure 2. Binding of (−)-GR24 and desmethyl germinone to D14L *in vitro*.

(**A**) Differential scanning fluorimetry (DSF) of MBP-His-D14L in the presence of 0–100 μM (−)-GR24 (left) or desmethyl germinone (dMGer) (right). Melting curves of the protein incubated with the indicated concentrations of each compound are shown in different colors. Each line represents a single replicate (triplicates for each concentration). Control experiments, in which the protein was incubated without KL analogs, are shown in both plots.

(**B**) Inhibitory effects of dMGer and (−)-GR24 on dYLG hydrolysis by MBP-6×His-D14L. Reactions contained 1 μM dYLG, 10 ng/μL protein, and the indicated concentrations of (−)-GR24 or dMGer. Dimethyl sulfoxide without either compound served as the mock control. Circles represent individual data points, expressed relative to the mean fluorescence intensity of mock reactions; bars indicate means (n = 4).

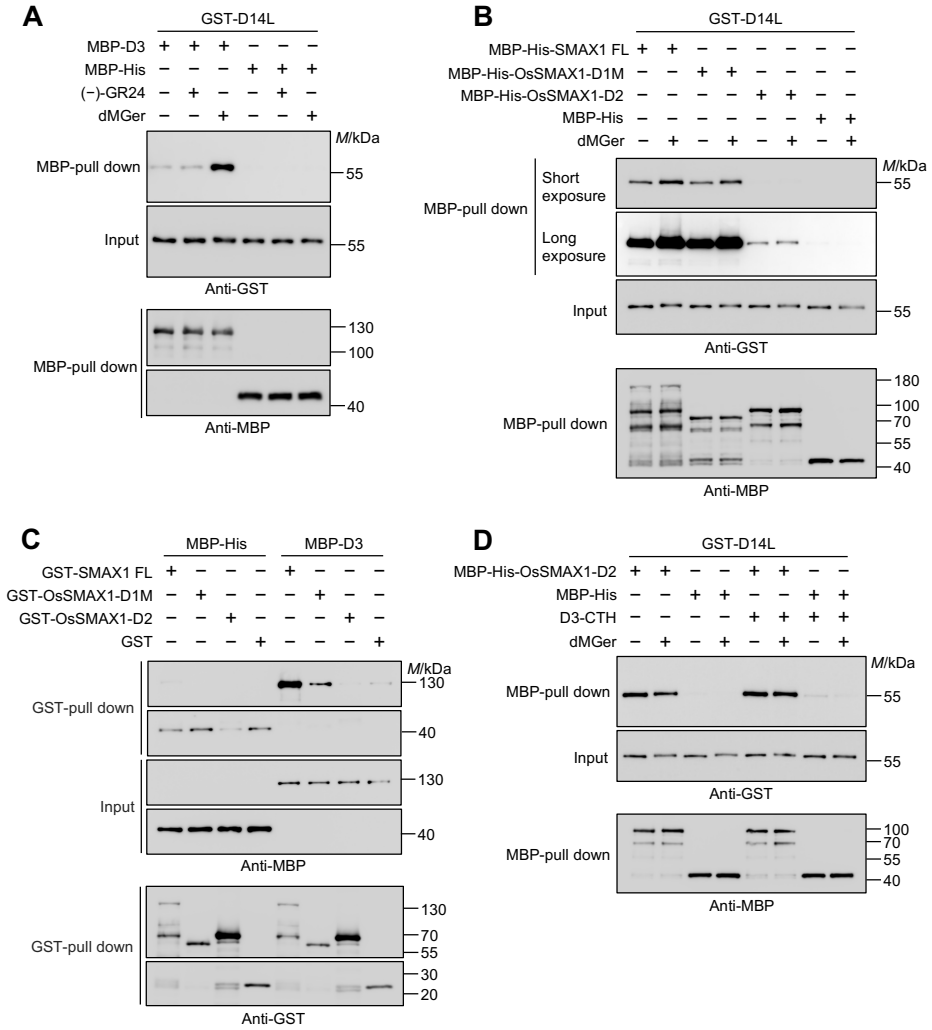

Figure 3. Interactions between KL-signaling components.

(**A**) *In vitro* MBP pull-down assay using dextrin agarose beads, with MBP-D3 co-expressed with ASK1 or MBP-His tag alone as bait, and GST-D14L as prey. All reactions contained 0.2% (v/v) DMSO as solvent for chemicals. Assays were supplemented with either 10 μM dMGer, 10 μM (−)-GR24, or DMSO only. Calculated molecular masses: GST-D14L, ~56 kDa; MBP-D3, ~121 kDa; MBP-His tag, ~45 kDa.

(**B**) *In vitro* MBP pull-down assay using MBP-His-tagged full-length (FL) or domain fragments of OsSMAX1 as bait, and GST-D14L as prey. Assays were performed with or without 10 μM dMGer. For better visualization of GST-D14L pulled-down by each bait, images of the same blot taken with different exposure times (short and long) are shown. Calculated molecular masses: MBP-His-OsSMAX1 FL, ~154 kDa; MBP-His-OsSMAX1-D1M, ~79 kDa; MBP-His-OsSMAX1-D2, ~90 kDa.

(**C**) *In vitro* GST pull-down assay using glutathione agarose beads, with GST-tagged FL or domains of OsSMAX1 as bait, and MBP-D3 or MBP-His as prey. Calculated molecular masses: GST-OsSMAX1 FL, ~135 kDa; GST-OsSMAX1-D1M, ~60 kDa; GST-OsSMAX1-D2, ~71 kDa; GST tag, ~28 kDa.

(**D**) *In vitro* MBP pull-down assay using MBP-His-OsSMAX1-D2 as bait and GST-D14L as prey, performed in the presence or absence of D3-CTH peptide, with or without 10 μM dMGer.

GST- and MBP(-His)-tagged proteins were detected by immunoblotting with anti-GST and anti-MBP antibodies, respectively. The positions of size markers electrophoresed with the samples are shown alongside each blot.

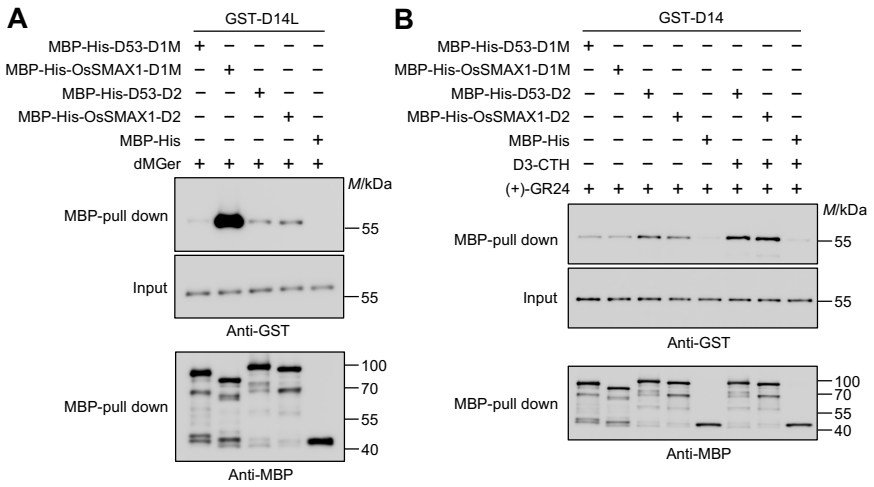

Figure 4. Differential interaction of D14L and D14 with domains of OsSMAX1 and D53. (**A**) *In vitro* MBP pull-down assay using MBP-His-tagged domains of D53 or OsSMAX1 as bait, and GST-D14L as prey. All reactions contained 10 μM dMGer. Calculated molecular masses: MBP-His-D53-D1M, ~80 kDa; MBP-His-D53-D2, ~91 kDa.

(**B**) *In vitro* MBP pull-down assay using MBP-His-tagged domains of D53 or OsSMAX1 as bait, and GST-D14 as prey, performed in the presence or absence of D3-CTH. All reactions contained 10 μM (+)-GR24. Calculated molecular masses: GST-D14 ~56 kDa.

GST- and MBP-His-tagged proteins were detected by immunoblotting with anti-GST and anti-MBP antibodies, respectively. The positions of size markers electrophoresed with the samples are shown alongside each blot.

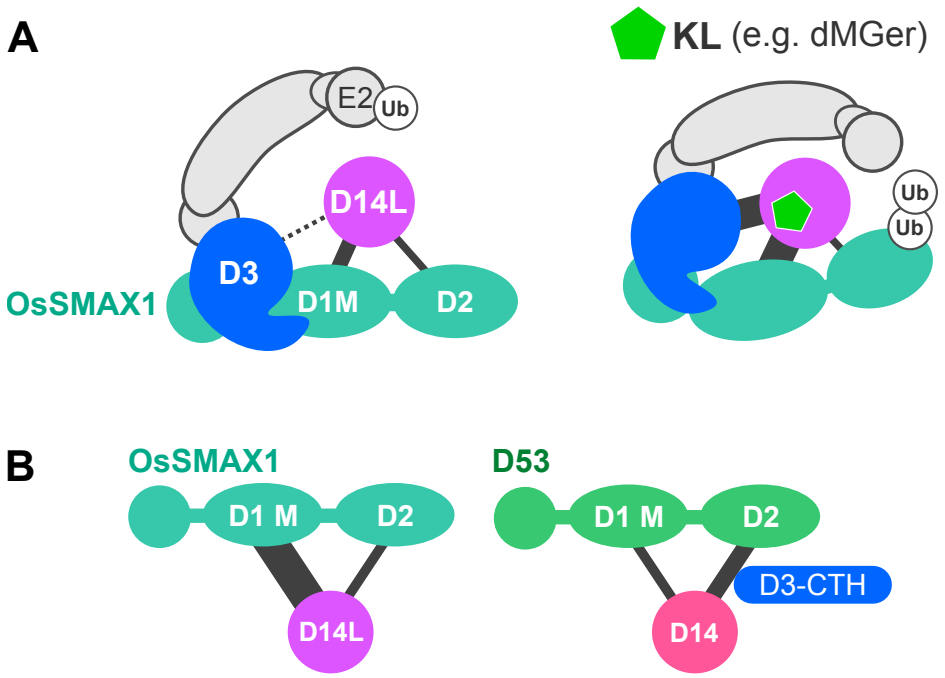

Figure 5. Interactions between rice KL-signaling components and effects of KL.

(**A**) Model of KL-triggered changes in protein–protein interactions. Even in the absence of KL, OsSMAX1 interacts with both D14L and D3, potentially forming a single complex. KL promotes direct binding between D14L and D3 and enhances the interaction between D14L and OsSMAX1, likely stabilizing and altering the conformation of the complex, thereby leading to the ubiquitination of OsSMAX1. Differences in interaction strength are indicated by the thickness of grey lines.

(**B**) Schematic of physical interactions of rice D14L and D14 with domains of OsSMAX1 and D53. D14L mainly interacts with OsSMAX1-D1M, whereas D14 mainly interacts with D53-D2. D3-CTH enhances the interaction between D14 and the D53-D2 domain. Differences in interaction strength are indicated by the thickness of grey lines.